

Supporting Information

Persistent Triboelectrification-induced Electroluminescence for Self-Powered All-Optical Wireless User Identification and Multi-mode Anti-counterfeiting

Li Su,^a Zihan Wang,^e Chengyu Lu,^e Wenbo Ding,^e Yong Zhao,^a and Yunlong Zi^{*b,c,d}

- a. Hebei Key Laboratory of Micro-Nano Precision Optical Sensing and Measurement Technology, School of Control Engineering, Northeastern University at Qinhuangdao, Qinhuangdao, Hebei 066004, China
- b. Thrust of Sustainable Energy and Environment, The Hong Kong University of Science and Technology (Guangzhou), Nansha, Guangdong 511400, China
- c. HKUST Shenzhen-Hong Kong Collaborative Innovation Research Institute, Futian, Shenzhen, Guangdong, 518048 China
- d. Department of Mechanical and Aerospace Engineering, The Hong Kong University of Science and Technology, Clear Water Bay, Hong Kong SAR, China
- e. Tsinghua-Berkeley Shenzhen Institute, Shenzhen International Graduate School, Tsinghua University, Shenzhen 518055, China.

*Authors to whom correspondence should be addressed:

Prof. ZI, Yunlong, E-mail: ylzi@ust.hk

1. Experimental Section

Fabrication of SP-PTM

PDMS (Sylgard 184, Dow Corning) was treated as the matrix for EL phosphors ZnS:Cu, Al (Keyan) and persistent PL phosphors SAOED (Warners). Firstly, PDMS-based resin was mixed with 10% wt curing agent and a certain content of ZnS:Cu, Al. Then, the SAOED were uniformly dispersed in the above mixture with different weight ratios, which was coated onto a pre-treated acrylic substrate possessing a template with a specific size ($50\text{ }\mu\text{m} \times 50\text{ }\mu\text{m} \times 0.5\text{ mm}^3$). Subsequent curing at 80 °C for 2h, the film was peeled off from the substrate to obtain the luminescent layer. Afterward, a PZT ceramic (500 μm , Pant) layer was assembled at the bottom as the enhancement layer. Finally, the luminescent layer and enhancement layer were sandwiched by sticking two layers of 100 μm FEP together, for use as the electrification layer and the flexible substrate respectively. As a result, an all-in-one SP-PTM was obtained.

Fabrication of the MAD

Three kinds of commercial polyester screens were used for the screen-printing apparatus with a count of 100 mesh. Three types of screen patterns were prepared with small vertical strips and different arrangements to obtain different anti-counterfeiting information. The mixtures as mentioned above were printed on an acrylic substrate in sequence. Meanwhile, the corresponding printed layer was annealed at 80 °C for 2 hours following each screen-printing process. Finally, after the patterned cured elastomer was peeled with care, the substrate, PZT ceramic enhancement layer, and the electrification layer were followed by sequential constructing layer by layer. As a result, the produced MAD was obtained.

Characterizations

All SEM and EDS images were captured by field emission scanning electron microscope (Nova Nano 450, FEI). The crystal structure of phosphors was characterized by X-ray diffraction at room temperature (D8 Advance, Bruker AXS). PL emission and excitation spectra of SAOED were recorded by using a steady-state and transient-state fluorescence spectrometer (FLS-98, Edinburgh). The optical absorption was measured using a UV-Vis-NIR light source (UV-3600, Shimadzu). The

optical emission was observed using a spectrometer and a vertically arranged optical fiber collimating lens spectrometer (Nova, Idea optics). The TL curves of the phosphors were recorded with the assistance of a TL meter (Fj-417A, CNNC). The polarization-electric field (P - E) hysteresis loops of the PZT ceramic layer were measured at 1 kHz using a precision ferroelectric tester (Precision LC II, Radiant).

2. Supplementary Figures

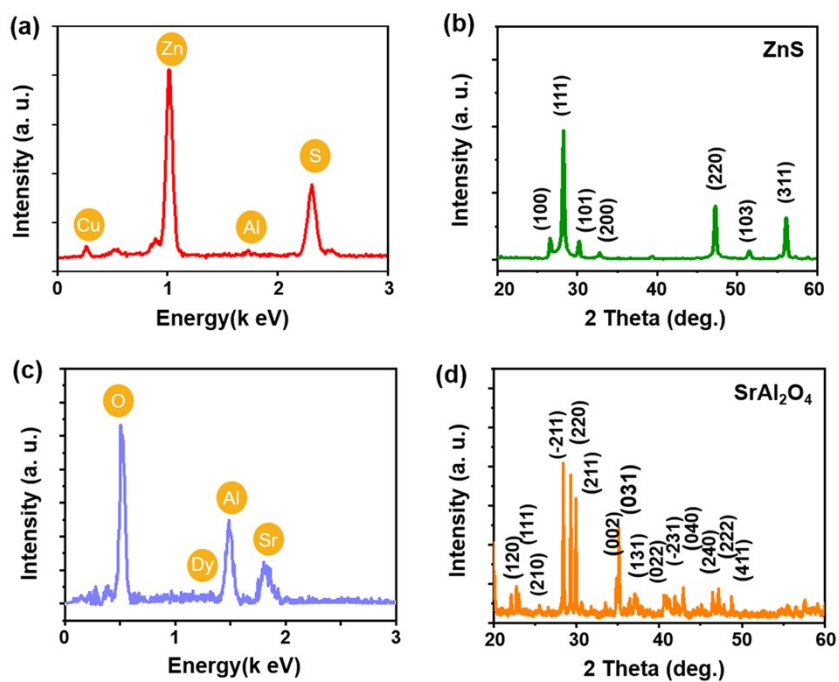


Figure S1. (a, b) XRD patterns and (c, d) EDS spectra of ZnS:Cu, Al and SAOED powders, respectively.

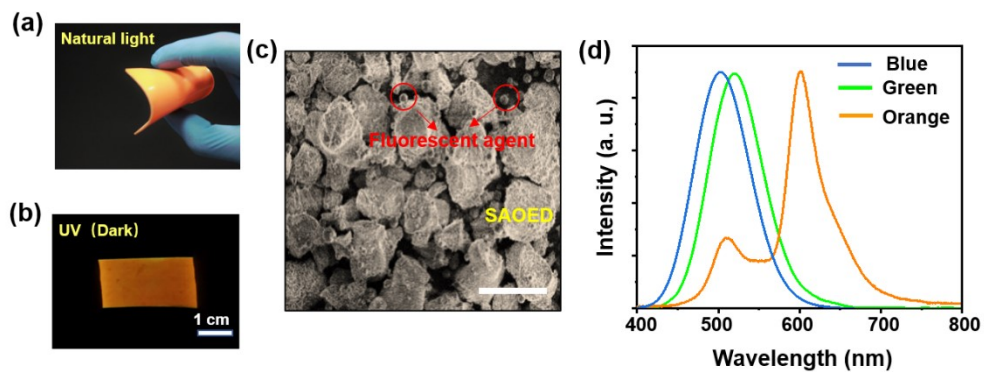


Figure S2. Optical photographs of the luminescent layer (orange light) under (a) natural lighting and (b) UV light irradiation in the dark condition. (c) SEM image of the SAOED incorporating the commercial fluorescent agent, scale bar: 30 μm . (d) TIEL spectra of SP-PTM with different luminescent colors: blue (phthalocyanine blue @SAOED), green, and orange (rhodamine B@SAOED).

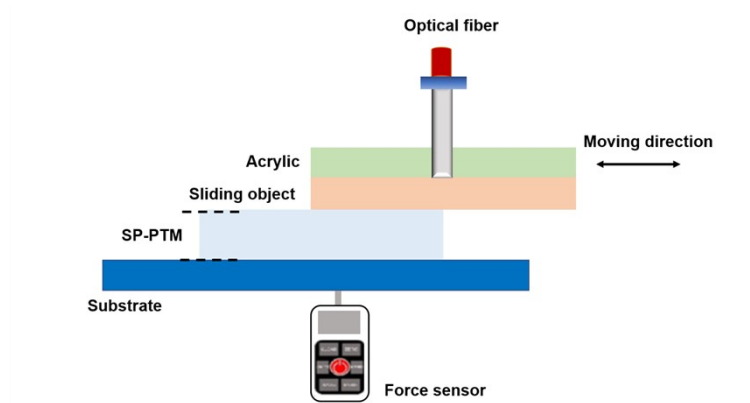


Figure S3. Schematic diagram of the test platform for measuring the TIEL emission, where a circular hole is designed to accommodate the optical fiber probe of the spectrometer.

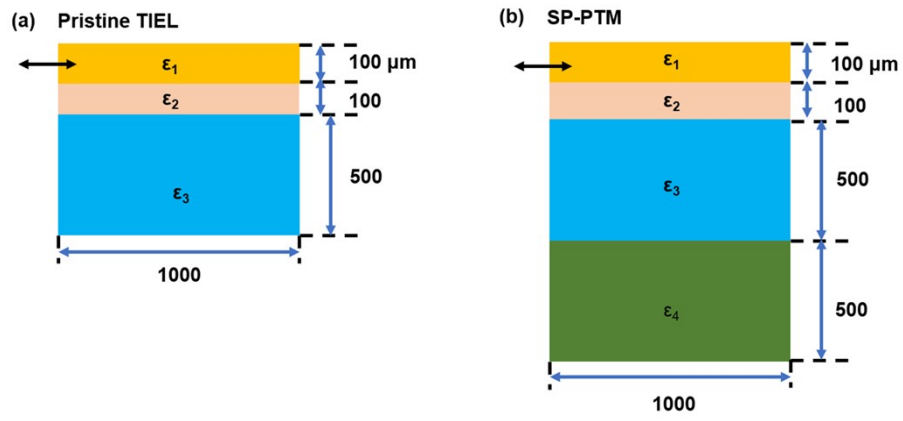


Figure S4. The 2D model setting of (a) pristine TIEL and (b) SP-PTM, respectively.

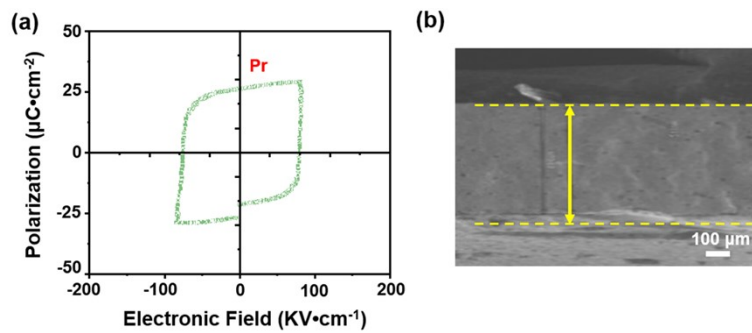


Figure S5. (a) P - E hysteresis loop and (b) Cross-sectional SEM micrograph for PZT ceramic layer.

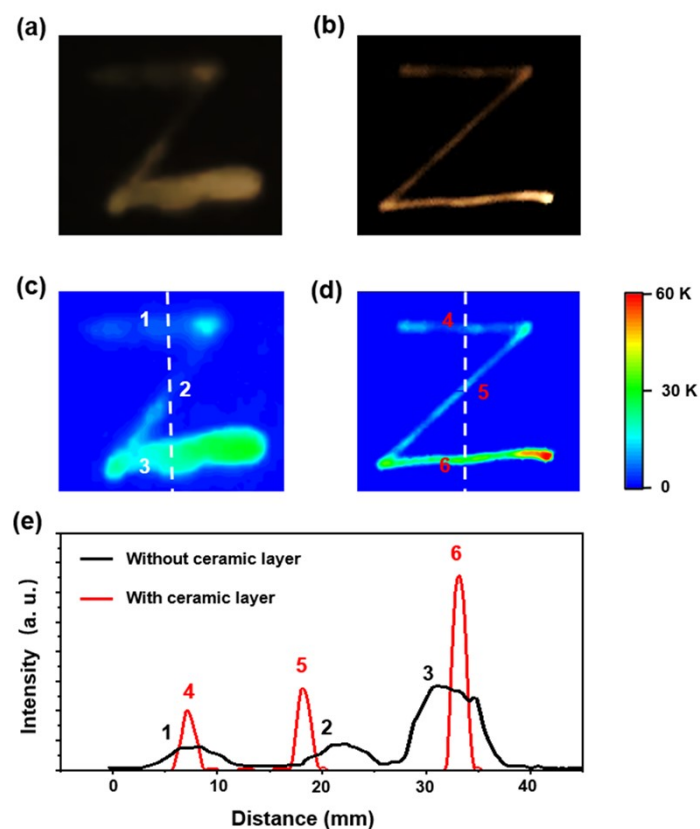


Figure S6. TIEL afterglow from the SP-PTM (a) without and (b) with a polarized ceramic layer. (c, d) Corresponding mapping of the luminescence intensity in (a) and (b). (e) Luminescence intensity distribution along the dashed lines defined in (c) and (d), indicating a distinct boundary and higher intensity from the SP-PTM with a polarized ceramic layer.

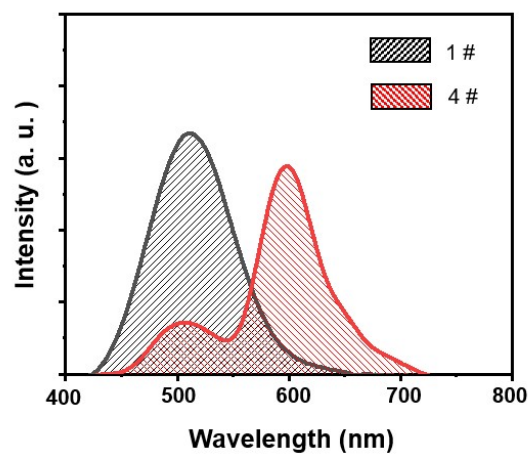


Figure S7. Measured TIEL spectra of sample 1# (black line) and 4# (red line) in Figure 3a. The conversion efficiency is calculated by dividing the spectrum curve area of the SP-PTM (sample 4#) by reference sample free of SAOED (sample 1#), which reaches as high as 85.3%.

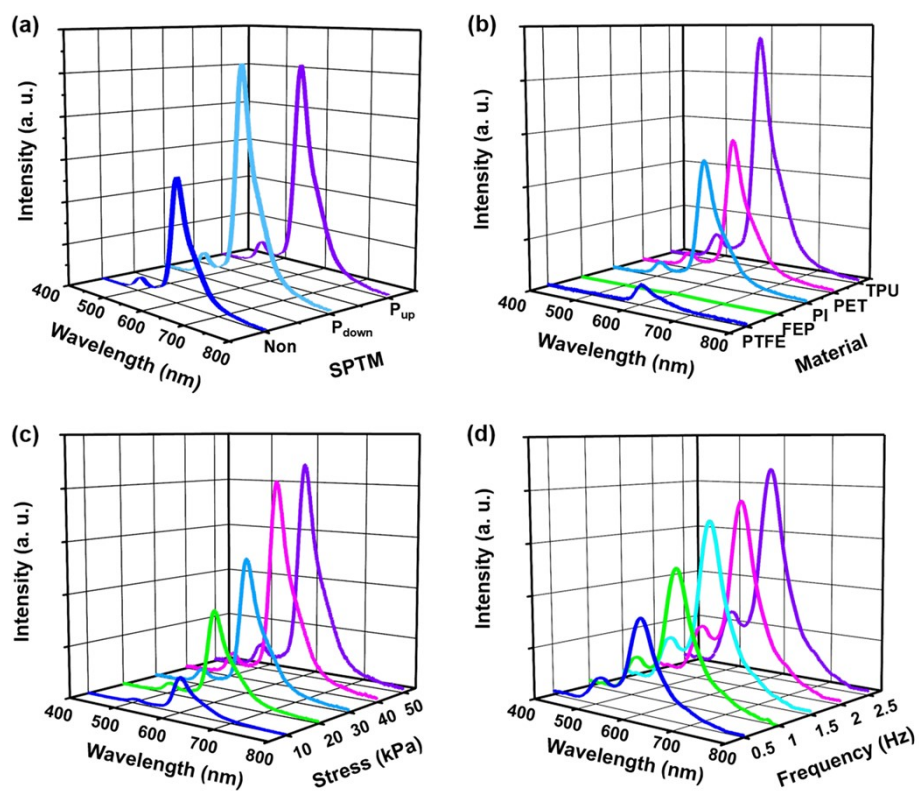


Figure S8. Dependence of TIEL spectra on (a) the PZT enhancement layer, (b) different materials as sliding objects, (c) increasing the applied stress from 10 to 50 kPa, and (d) increasing the frequency from 0.5 to 2.5 Hz.

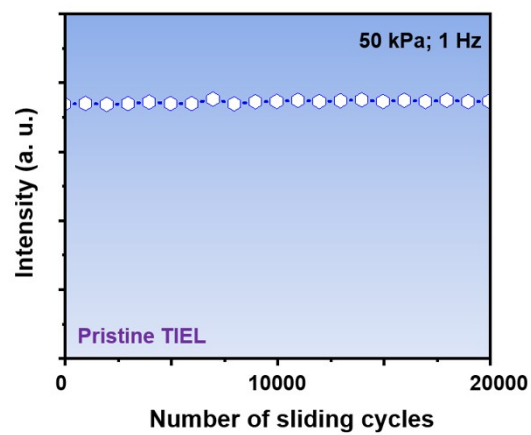


Figure S9. Stability and repeatability tests of pristine TIEL.

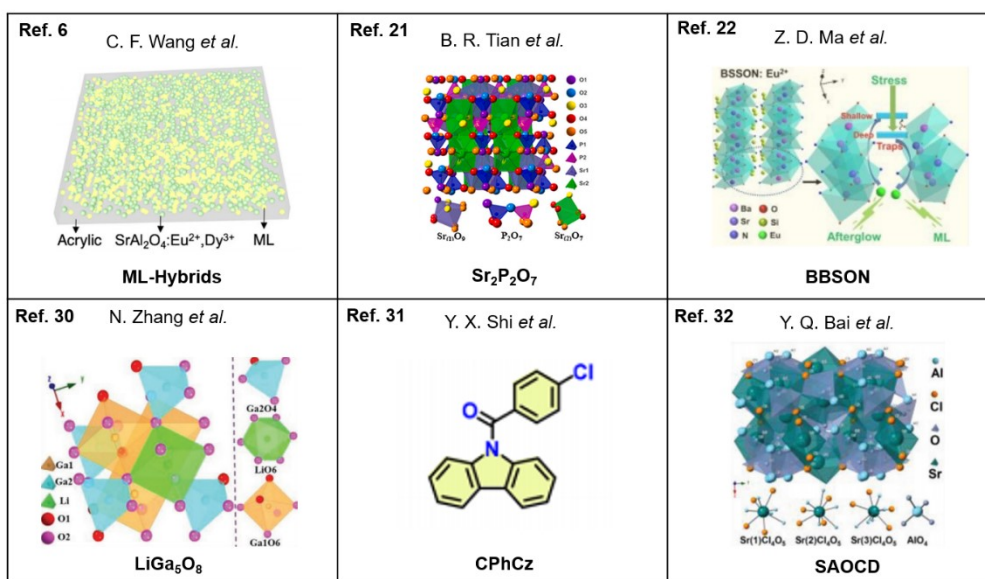


Figure S10. The chemical structures of the reported ML materials in Figure 4a.

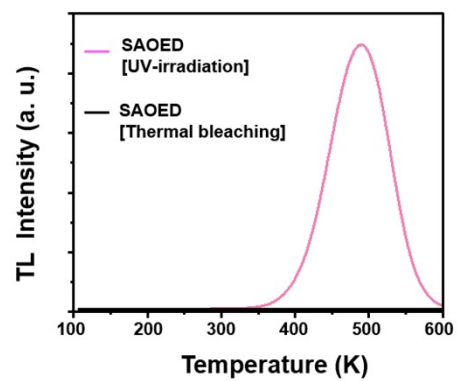


Figure S11. TL spectra of SAOED after the treatment of 365 nm UV light irradiation and thermal bleaching at 600 K for 5 min.

3. Supplementary Notes

Note S1. The COMSOL simulation.

The 2D models of pristine TIEL and SP-PTM were applied to demonstrate the distribution of electric field, as constructed in Figure S4. The PDMS matrix and the PZT ceramic layer had a size of $1000\ \mu\text{m} \times 500\ \mu\text{m}$. The thickness of the contact object was set to $100\ \mu\text{m}$. The charge density of the external object surface and electrification layer (FEP) was set to $30\ \mu\text{C}/\text{m}^2 (+\sigma_1)$ and $-30\ \mu\text{C}/\text{m}^2(-\sigma_1)$, respectively, while that of the upper and lower surfaces of the ceramic layer was set to $0.2\ \text{C}/\text{m}^2 (+\sigma_2)$ and $-0.2\ \text{C}/\text{m}^2 (+\sigma_2)$ according to the remnant polarization (Pr) as achieved through *P-E* hysteresis loop (Figure S3a), respectively. The dielectric permittivity used for simulation was $\epsilon = 1.0$ for air, $\epsilon_1 = 10.0$ for the external object, $\epsilon_2 = 2.1$ for FEP, $\epsilon_3 = 20.0$ for PDMS, and $\epsilon_4 = 2000$ for the PZT ceramic. The whole model was simulated in the presence of ambient air.

Note S2. The classification algorithm for user identification.

Our image classification algorithm is designed to distinguish the spatial distribution of luminescent trajectory generated by different users' sliding. The image classification algorithm consists of three parts, image pre-processing, image feature extraction, and classifier training.

The image pre-processing start from transforming the RGB images captured by the camera into greyscale images. Then we use the Otsu method to compute a threshold value that minimizes the weighted variance between the foreground and background pixels.¹ The optimum threshold value will be used for image binarization.

In the image feature extraction process, the Gray Level Co-occurrence Matrix (GLCM)² and the Histogram of Oriented Gradient (HOG)³ are utilized to extract global and local features of the pre-processed binary images, respectively. GLCM is a matrix that describes the distribution of co-occurring pixel values at a given offset, which focuses more on the macro information of an image. HOG is another feature descriptor that is frequently used in computer vision and image processing. It describes the features by computing the gradient direction histogram of the image's local regions. Specifically, the image will be divided into adjacent cells, and the gradient of the pixel inside the cell as well as the direction of pixels on the edge will be collected. The collected information will be used to constitute a histogram as the descriptor. Since the gradient mainly occurs on the edges, the HOG is more focused on the local characteristics of images.

We use the extracted features to train support vector machines (SVM) as the classifier.⁴ The main idea of SVM is to find the decision planes that define the decision boundary of two classes. Since our task requires the classification of multiple users, we adopt the on-versus-the-rest strategy to constitute a classifier.⁵ In the training stage, the feature from the user of interest is classified as a positive class and the features from the rest users are classified as a negative class. Such that, the classifier contains k models for k users. In order to handle the non-linear classification situation and improve the robustness of the models, we adopt the RBF kernel,⁶ also known as the Gaussian kernel, to train the model.

In the classification (inferencing) stage, the unknown input image will be pre-processed and extracted features. Here, we adopt the max-wins-voting strategy to realize the multi-class classification.⁷ Specifically, the features will input the classifier containing k models, each model will calculate a prediction score for a certain class, and the class with the highest score is considered the prediction result.

References

- 1 N. Otsu, *IEEE transactions on systems, man, and cybernetics*, 1979, **9**, 62-66.
- 2 H. Bo, F. L. Ma and L. C. Jiao, *Acta Electronica Sinica*, 2006, **34**, 155.
- 3 Y. Tanaka and T. Kengo, 2009 10th international conference on document analysis and recognition, October, Barcelona, Spain, 2009.
- 4 C. Corinna and V. Vapnik, *Machine learning*, 1995, **20**, 273.
- 5 J. Weston and W. Chris, Technical Report CSD-TR-98-04, Department of Computer Science, May, University of London, England, 1998.
- 6 M. Ring and E. M. Bjoer, *Pattern Recognition Letters*, 2016, **84**, 107-113.
- 7 C. W. Hsu and C. J. Lin, *IEEE transactions on Neural Networks*, 2002, **13**, 415-425.